NASA Technical Memorandum 101402

Oxidation Behavior of FeAl + Hf,Zr,B

James L. Smialek
National Aeronautics and Space Administration
Lewis Research Center
Cleveland, Ohio

Joseph Doychak
Sverdrup Technology, Inc.
NASA Lewis Research Center Group
Cleveland, Ohio

and

Darrell J. Gaydosh
National Aeronautics and Space Administration
Lewis Research Center
Cleveland, Ohio

Prepared for the
Workshop on the Oxidation of High-Temperature Intermetallics
sponsored by the Cleveland Chapter of ASM International and NASA Lewis Research Center in cooperation with Case Western Reserve University, The Metallurgical Society of AIME, and the Cleveland Chapter of TMS-AIME
Cleveland, Ohio, September 22–23, 1988

NASA

OXIDATION BEHAVIOR OF FeAl+Hf,Zr,B

James L. Smialek
National Aeronautics and Space Administration
Lewis Research Center
Cleveland, Ohio 44135

Joseph Doychak
Sverdrup Technology, Inc.
NASA Lewis Research Center Group
Cleveland, Ohio 44135

and

Darrell J. Gaydosh
National Aeronautics and Space Administration
Lewis Research Center
Cleveland, Ohio 44135

Abstract

The oxidation behavior of Fe-40Al-1Hf, Fe-40Al-1Hf-0.4B, and Fe-40Al-0.1Zr-0.4B (at %) alloys was characterized after 900°, 1000°, and 1100 °C exposures. Isothermal tests revealed parabolic kinetics after a period of transitional θ-alumina scale growth. The parabolic growth rates for the subsequent α-alumina scales were about five times higher than those for NiAl+0.1Zr alloys. The isothermally grown scales showed a propensity toward massive scale spallation due to both extensive rumpling from growth stresses and to an inner layer of HfO_2. Cyclic oxidation for 200 1-hr cycles produced little degradation at 900 or 1000 °C, but caused significant spallation at 1100 °C in the form of small segments of the outer scale. The major difference in the cyclic oxidation of the three FeAl alloys was increased initial spallation for FeAl+Zr,B. Although these FeAl alloys showed many similarities to NiAl alloys, they were generally less oxidation resistant. It is believed that this resulted from nonoptimal levels of dopants and larger thermal expansion mismatch stresses.

Introduction

Fe-40Al (at % unless otherwise noted) is an intermetallic compound currently being considered as a matrix for high temperature fiber reinforced composites. Its primary advantages over other intermetallics are high ductility (1 to 5 percent) and low cost. It maintains a yield strength of about 500 MPa up to 500 °C, decreasing to 60 MPa at 827 °C (1). It has a relatively low melting point (1340 °C) and high coefficient of thermal expansion (21×10^{-6}/°C) compared to NiAl (1650 °C and 16×10^{-6}/°C). This material will thus be competitive only at temperatures below 1000 °C, especially when used in conjunction with low expansion fibers, such as Al_2O_3 (9.5×10^{-6}/°C).

Aluminides are generally considered to be oxidation resistant because of their ability to form protective alumina scales. However some minimum amount of aluminum is required to insure this. Hagel found exclusive α-Al_2O_3 scales after 10 hr oxidation of Fe-22Al (12 wt %) above 1000 °C (2). However another study found that 30 at % aluminum was required to produce slow growth kinetics indicative of alumina scales at 900°, 1000°, and 1100 °C (3). Based on this data, Fe-40Al is also expected to be an alumina former. Hagel also found that a transition occurred from γ-Al_2O_3 to α-Al_2O_3 between 900° and 1050 °C, accompanied by a substantial drop in oxidation kinetics.

Cyclic oxidation screening studies were performed on a number of Fe-40Al-5X and Fe-45Al-5X alloys at 1200 °C, where X = Ti, Cr, Co, Ni, Zr, Nb, Mo, Ta, W, or Re. (unpublished data of C.A. Barrett, R.H. Titran, NASA Lewis, 1985). Acceptable performance nearly equal to the unalloyed binary compounds (2 to 5 mg/cm^2 weight loss after 200 1-hr cycles) was achieved for Cr, Re, and Nb additions to Fe-45Al and for Ni additions to Fe-40Al. Marginal performance (10 to 35 mg/cm^2 weight loss) was achieved for Ti, Ni, and Co additions to Fe-45Al and for Si additions to Fe-40Al. Very poor behavior occurred for Zr, Mo, Ta, and W additions to Fe-45Al.

The present study follows upon this work to some degree in that one of the key recommendations was to lower the amount of oxygen-active elements usually required for scale adhesion (e.g. Hf or Zr). Thus Hf was added at a 1 at % level. Zr was added at a 0.1 at % level because of the excellent oxidation resistance of NiAl-0.1Zr (4). Both dopants are known getters of O and S and consequently help prevent creep cavitation (5). Boron is well known to eliminate low temperature intergranular fracture in Ni_3Al (6).

Our purpose in this work was to characterize the 900°, 1000°, and 1100 °C isothermal and cyclic oxidation behavior of Fe-40Al-1Hf, Fe-40Al-1Hf-0.4B, and Fe-40Al-0.1Zr-0.4B alloys. These three specific alloys were chosen only because they are the focus of a parallel program investigating the mechanical properties of FeAl composites (7). The kinetic and microstructural observations are compared to NiAl alloys for which a good understanding and strong data base already exists.

Experimental Procedure

Alloys were produced by hot extruding vacuum sealed cans of gas atomized prealloyed powders at 977 °C with an area reduction of 16:1 (7). Boron was preblended as an elemental powder and resulted in an inhomogeneous distribution. Alloy compositions were Fe-40Al-1Hf, Fe-40Al-1Hf-0.41B and Fe-40Al-0.1Zr-0.41B (at %). Major impurities were Ta, Co, Cr, Ni, and Mn totalling less than 0.5 percent. O, C, and S were present at 500, 35, and 30 ppmw, respectively. Test specimens were sectioned and

machined to 0.65 x 0.65 x 2.5 cm dimensions and polished to a 600 grit finish. Isothermal oxidation was performed in a Cahn 1000 microbalance for 140 hr. Cyclic oxidation was performed for 200 hr with 1-hr heating/ 20 min cooling cycles. Both exposures were in 1 atm air at 900°, 1000°, and 1100 °C. Characterization was made by XRD, SEM/EDS, and optical metallography.

Results and Discussion

Oxidation Kinetics and Scale Phases

Parabolic rate constants were estimated from weight change versus $(time)^{1/2}$ plots for the three alloys and temperatures. The results are shown in the Arrhenius plot of Fig. 1. Relatively high values were obtained for the 900 °C runs and are believed to be due to the formation of transition aluminas having higher growth rates. The three alloys are comparable to the 900 °C data for θ-Al_2O_3 growth rates found for NiAl+Zr (8). The higher temperature data appears to fall in a band about a factor of five above that for all published data for α-Al_2O_3 growth on NiAl (8).

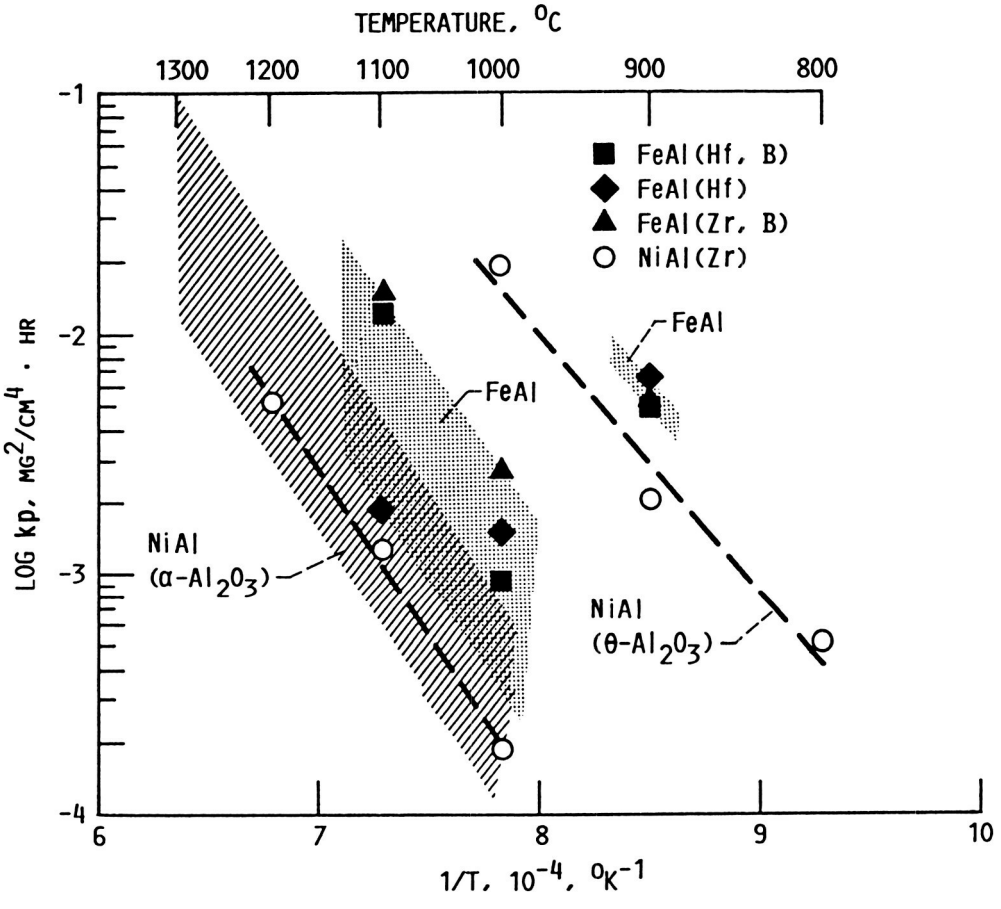

Figure 1. - Arrhenius plot comparing FeAl and NiAl oxidation kinetics. (NiAl data from ref. 8).

Table I shows that α-Al_2O_3 was the predominant scale phase produced by isothermal oxidation. However some peaks consistent with θ-Al_2O_3 were observed, especially at lower temperatures. Correspondence with the two curves in Fig. 1 and the transition to a different scale phase is similar to the γ-α transition reported by Hagel (2). Hf-containing alloys may also have had some Fe_2O_3 present in solid solution with α-Al_2O_3, as the measured lattice parameter was slightly enlarged by 0.8 percent.

TABLE I. - SUMMARY OF SCALE PHASES AFTER ISOTHERMAL (140 hr) AND CYCLIC (200 1-hr CYCLES) OXIDATION

[α = α-Al_2O_3; θ = θ-Al_2O_3; α+ = α-$(Al,Fe)_2O_3$; HfO_2 = Monoclinic HfO_2; ( ) = weak pattern.]

Alloy	Isothermal			Cyclic		
	900	1000	1100	900	1000	1100
FeAl+Hf	α, θ	α, (θ) +	α, (θ) +	α, HfO_2	α, HfO_2	α, HfO_2
FeAl+Hf, B	α, θ	α, (θ) +	α, (θ) +	α	α	α, HfO_2
FeAl+Zr, B	α	------	α	θ	α	α

The cyclic oxidation results are shown in Fig. 2. The 900 °C curves show moderate weight gains of 0.25 to 0.35 mg/cm^2 after 200 hr, with no obvious signs of scale spallation (Fig. 2a). Interestingly enough, the 0.1 percent Zr alloy exhibited higher weight gain compared to the 1 percent Hf alloys. This is in contrast to the usual observation of higher weight gains for larger amounts of oxygen-active dopants. At 1000 °C the Hf-containing alloys show small weight changes (Fig. 2b). However, the Zr-doped alloy now shows some weight loss due to spalling which was observed visually in the form of an extremely fine dusting. Oxidation at 1100 °C also produced dusting for all three alloys. The Hf-containing alloys did not show negative slopes in the weight change curves until well past 100 cycles, whereas the Zr-doped alloy lost weight rapidly from the very first cycle (Fig. 2c). The scale phases produced by cyclic oxidation were primarily α-Al_2O_3, plus some HfO_2 for the Hf-containing alloys (Table I).

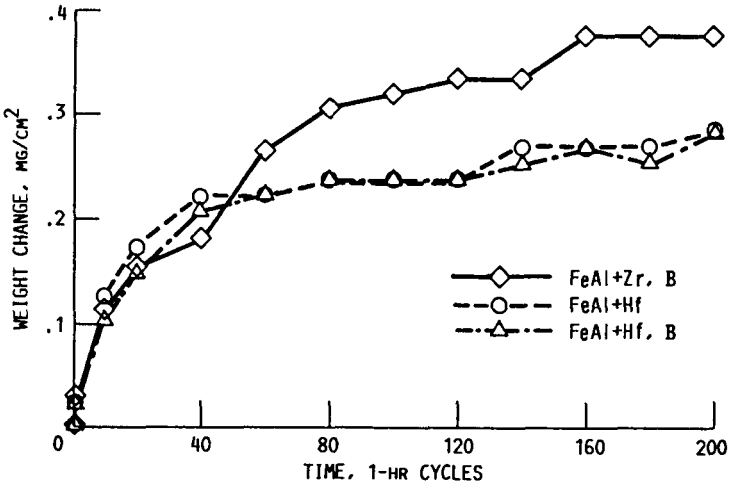

Figure 2. - Gravimetric curves for cyclic oxidation of Fe-40Al alloys for 200 1-hr cycles: (a) 900 °C, (b) 1000 °C), (c) 1100 °C.

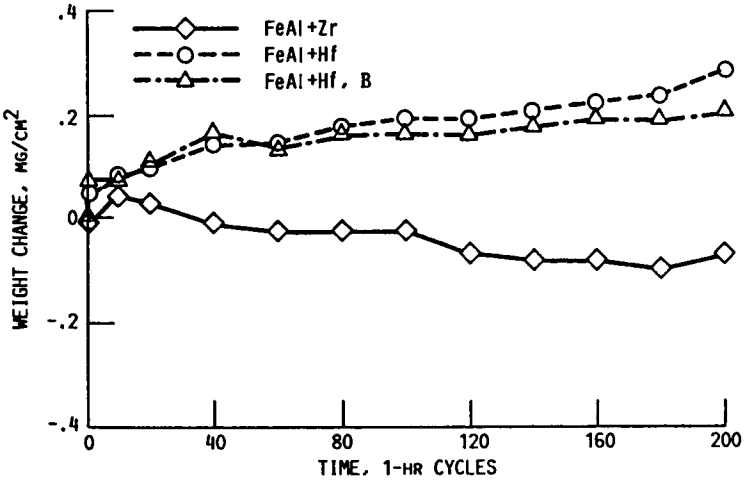

FIGURE 2b.

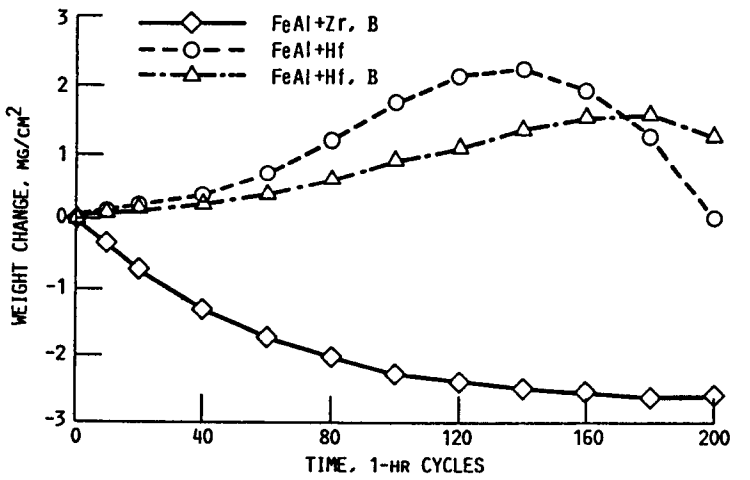

FIGURE 2c.

Scale Microstructures

The scale microstructures varied considerably with oxidation treatment and alloy composition. In many cases these changes can be correlated with changes in the scale phase, growth kinetics, and spalling characteristics. The isothermal structures will be described first.

FeAl+Hf, isothermal. At 900 °C this alloy formed a distinct whisker morphology with a distribution of shallow depressions (Fig. 3). Such scales have also been observed for 900 °C oxidation of NiAl+Zr under the same conditions (8). In both cases the whisker morphology was associated with a fast-growing θ-phase transition alumina. Oxidation at 1000 °C produced spheroidization and coarsening of any residual whisker morphology and the appearance of concave cells (Fig. 4). Further coarsening took place at 1100 °C, as the cells were flattened and occupied the majority of the surface (Fig. 5). At the cell boundaries, a hint of ridge network can be seen, reminiscent of the distinctive networks commonly observed for NiAl. Some radial crack-like features are also visible within these cells.

900 °C, ISOTHERMAL

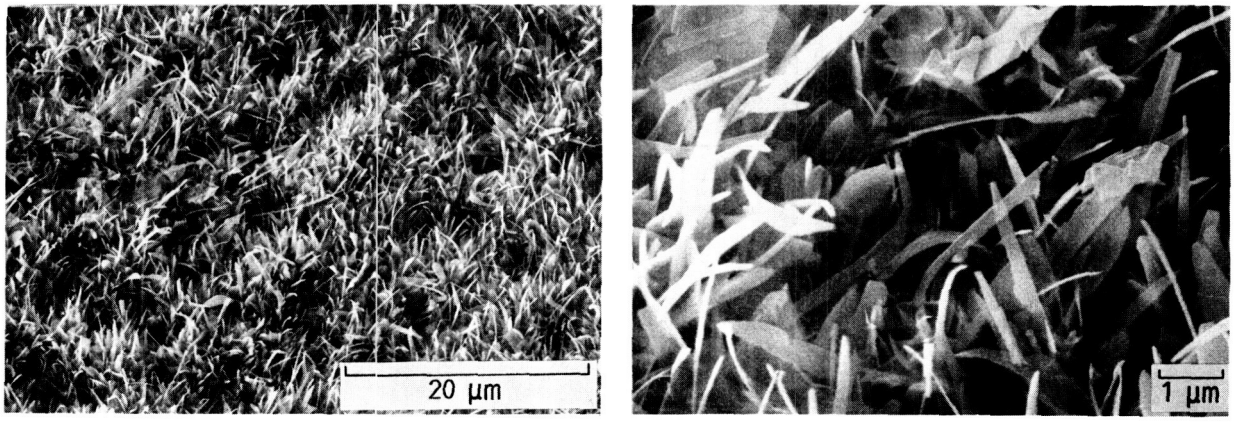

θ - Al_2O_3 WHISKER FORMATION

Figure 3. - θ-Al_2O_3 whiskers and depressions formed on FeAl-Hf (900 °C), isothermal).

1000 °C, ISOTHERMAL

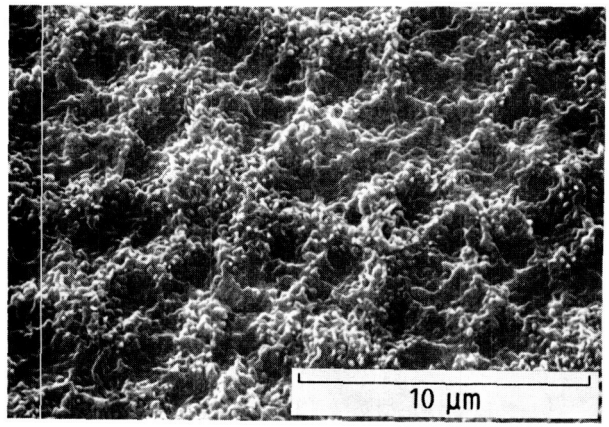

CELLULAR STRUCTURE

Figure 4. - Cellular depressions and nodules formed on FeAl+Hf (1000 °C, isothermal).

1100 °C, ISOTHERMAL

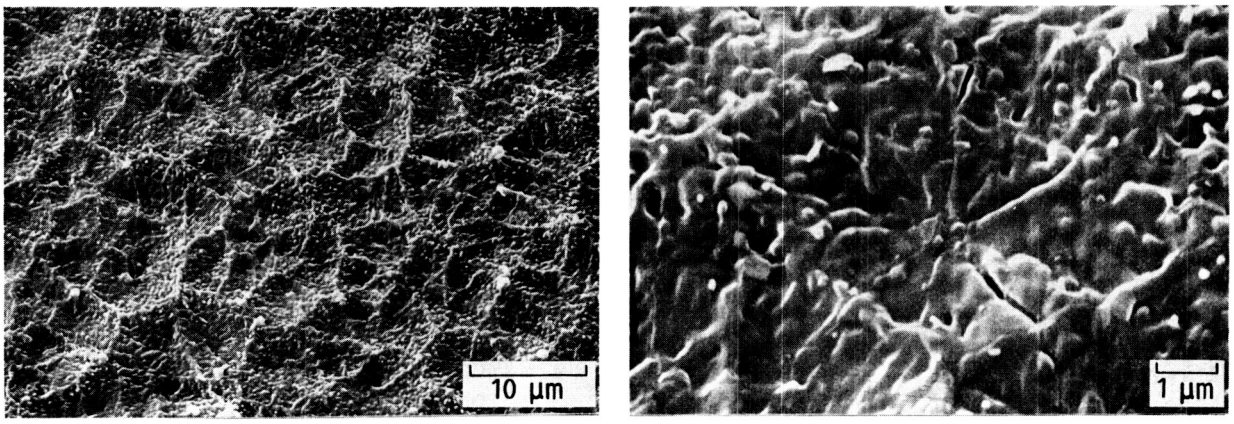

CELLS, RIDGES, AND TRANSFORMATION CRACKS

Figure 5. - Cells, ridge networks, and radial cracks formed on FeAl+Hf (1100 °C, isothermal).

This sequence of microstructures has been described in detail for the case of NiAl+Zr, and the resultant ridge network is described schematically in Fig. 6. (8,9). At low temperatures and for short times, the scales are metastable cubic phases of alumina which eventually transform to α-Al_2O_3 in the form of nucleation cells. This transformation produces a 14 percent volume contraction causing radial cracks in the cells. The last portions to transform are the regions between cells. These regions are thicker because they have experienced considerable outward scale growth, i.e., fast cation diffusion both in the metastable cubic alumina phases initially present and in the high angle grain boundaries remaining after the transformation is complete.

T = 1000 °C - 1200 °C, AIR, 100 HOURS

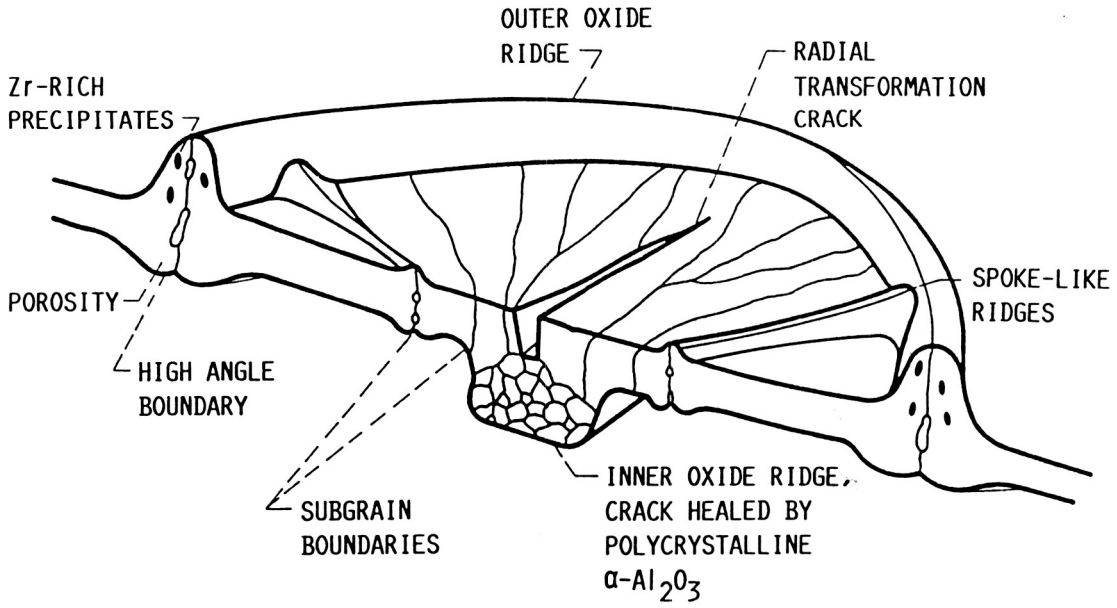

Figure 6. - Schematic section of ridge features from STEM studies of NiAl oxidation. (after Doychak, ref. 9).

A few small regions of localized spalling to bare metal occurred for the 1100 °C FeAl+Hf specimen. These areas revealed smoothed interface voids in the metal, dotted with Hf-rich particles, presumably HfO_2.

FeAl+Hf,B, isothermal. 900 °C isothermal oxidation of this alloy also produced a whisker morphology with a scattering of depressions. At 1000 °C the whisker and cellular structure was absent. Instead, a relatively uniform distribution of fine, 0.1 to 2.0 μm nodules decorated the polishing marks. This lack of whisker growth may explain the low k_p observed for this alloy at 1000 °C (Fig. 1). Oxidation at 1100 °C produced tremendous wrinkling, cracking, and spalling of the scale after cooling (Fig. 7). The spalled regions, apparent as the bright features in the backscatter image, were usually not to bare metal but exposed a layer of hafnium oxide as surmised from strong Hf EDS peaks. Some of these regions contained just a few Hf-rich particles, as found on the FeAl+Hf alloy.

FeAl-1Hf-0.4B; 1100 °C, ISOTHERMAL

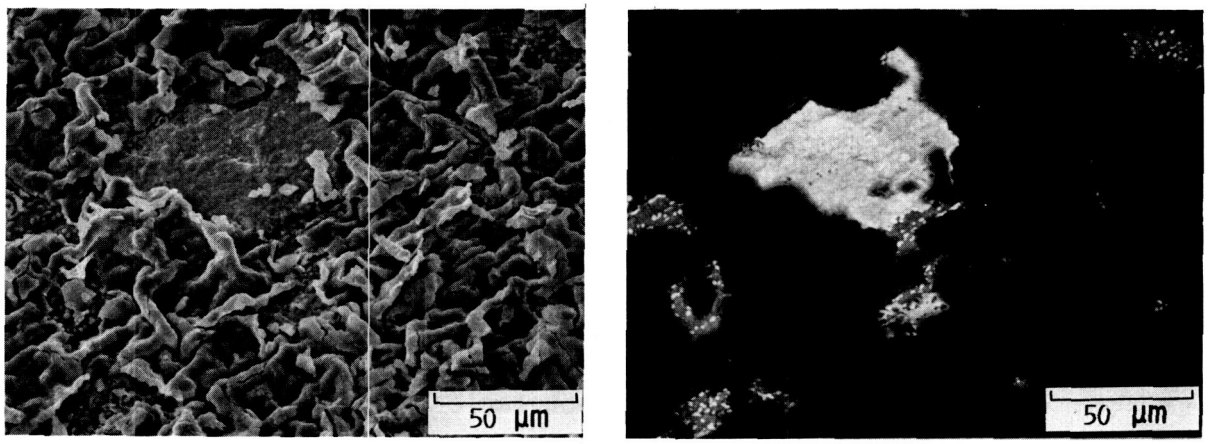

SECONDARY ELECTRON BACKSCATTER

Figure 7. - Convolutions and interfacial spalling for FeAl+Hf,B (1100 °C, isothermal): (a) secondary electron image, (b) HfO_2 layer and particles in corresponding backscatter image.

FeAl+Zr,B, isothermal. This alloy produced the same whisker morphology at 900 °C as did the Hf-doped alloys, along with massive spalling to bare metal after cooldown. Spalled regions revealed extensive porosity in the metal interfacial layer. A whisker morphology with a high density of concave depressions (cf. Figs. 3 and 4). was produced by 1000 °C oxidation. These scales spalled as well, and the scale underside contained a high density of Zr-rich particles. Complete spallation also took place after oxidation and cooldown from 1100 °C. These scales, shown in Fig. 8, were highly convoluted, as was the case for the other boron-doped alloy (Fig. 7). Zr-rich particles were also noted on the exposed metal surface.

A summary of the morphological observations is given in Table II. For isothermal exposures, it is seen that the trend with increasing temperature is from whiskers to cells to ridges or buckled scales. The Zr-doped alloy spalled extensively at all three temperatures, while the Hf,B doped alloy spalled only at 1100 °C. Severe spalling to bare metal due to interfacial voidage had also been noted for undoped Ni-40Al after isothermal exposures (10). Nevertheless this alloy maintained good cyclic oxidation resistance at 1100 °C. Isothermal oxidation also produced spalling to bare metal for a 0.1Zr doped Ni-50Al due to interfacial voidage, but only above 1300 °C (13).

1100 °C, ISOTHERMAL

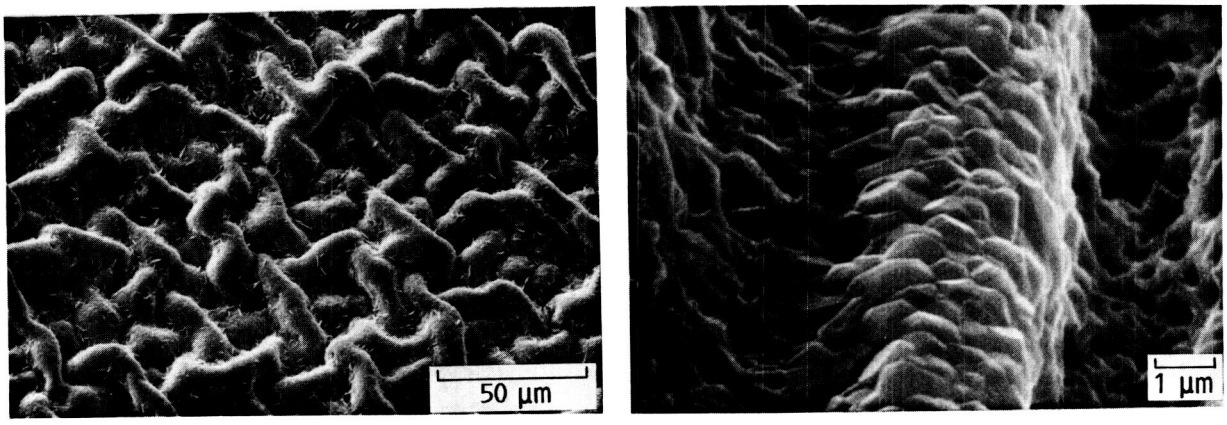

SPALLED SCALE, SEVERELY BUCKLED

Figure 8. - Convolutions in scale detached from FeAl+Zr,B (1100 °C, isothermal).

TABLE II. - SUMMARY OF SEM STUDIES

	Isothermal		
	Temperature, °C		
	900	1000	1100
FeAl-1Hf	Whiskers	Cells	Cells, ridges, cracks
FeAl-1Hf-0.4B	Whiskers	Fine nodules	Buckling, spalling at HfO_2 layer
FeAl-0.1Zr-0.4B	Whiskers, spalling at metal	Cells, whiskers, spalling at metal, ZrO_2 particles	Buckling, spalling at metal
	Cycles		
FeAl-2Hf	Platelets	Fine nodules	Fragments, HfO_2 in oxide
FeAl-1Hf-0.4B	Whiskers	Nodules	Fragments, HfO_2 in oxide
FeAl-0.1Zr-0.4B	Whiskers	Fragments, buckling	Fine spall fragments

FeAl+Hf, cyclic. Cyclic oxidation produced little spallation at 900 °C, thus the microstructure was basically the same as that produced by isothermal oxidation (Table II). The only difference was a few regions of spalling and more of a platelet than whisker texture. The 1000 °C sample was flat and featureless compared to the cellular nature of the isothermal case in Fig. 4. Only some very fine nodules were apparent. At 1100 °C the differences became more noticeable. The scale was extensively damaged by cracking and spalling of segments, with fracture occurring primarily within the scale (Fig. 9). This damage explains the decidedly downward trend in weight change at the end of the cyclic test (Fig. 2). Backscatter imaging revealed stringers of high atomic number precipitates within the alumina (Figs. 9 and 10), which were concluded to be HfO_2 by EDS and XRD. The formation of these particles was associated with the oxidation of Hf-rich precipitates in the alloy, resulting in a depletion zone near the surface (Fig. 11). The precipitates had previously been identified as Al_6Fe_6Hf using TEM (11).

FeAl+Hf,B, cyclic. This alloy showed cyclic oxidation morphologies identical to those just described for FeAl+Hf, that is, whiskers plus platelets, flat structure, and spall fragments at 900°, 1000°, and 1100 °C, respectively. However it appears to have begun spalling earlier than did FeAl+Hf (Fig. 2c), consistent with the rumpling and decohesion found isothermally (Fig. 7a).

1100 °C, CYCLIC

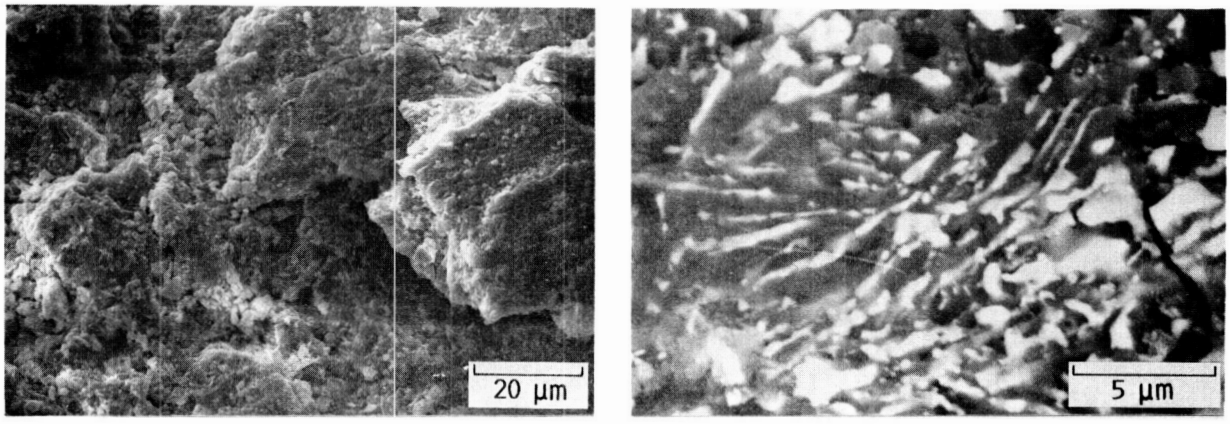

SECONDARY ELECTRON BACKSCATTER

FRAGMENTED SCALE, HfO_2 STRINGERS WITHIN SCALE

Figure 9. - Spall fragments and HfO_2 stringers in scale formed on FeAl+Hf (1100 °C, cyclic): (a) secondary electron image, (b) backscatter electron image of fragment in part a.

1100 °C, CYCLIC

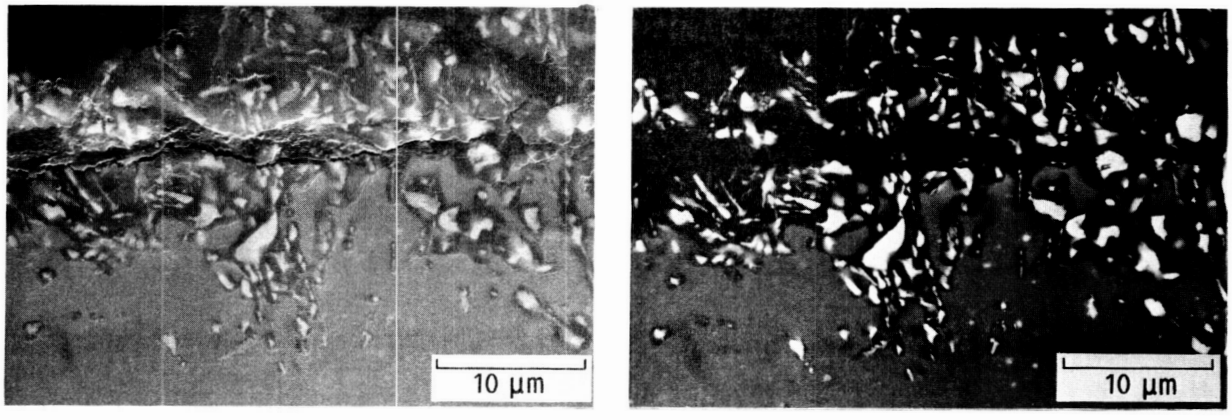

SECONDARY ELECTRON BACKSCATTER

HfO_2 STRINGERS IN EXTERNAL SCALE AND IN ALLOY

Figure 10. - Internal and external HfO_2 stringers in a cross-section of FeAl+Hf (1100 °C, cyclic): (a) secondary electron image, (b) corresponding backscatter electron image.

1100 °C, CYCLIC

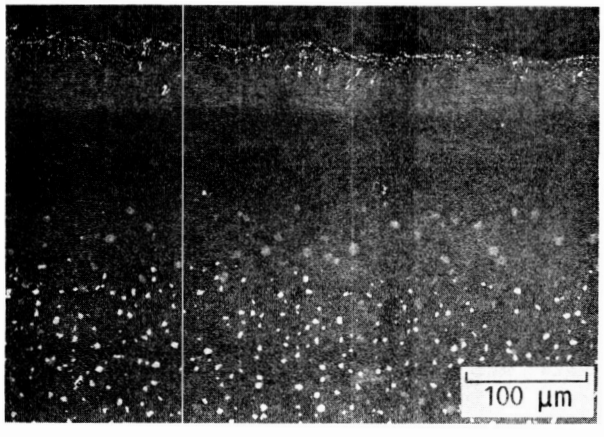

← $Al_2O_3 + HfO_2$

DEPLETION ZONE

Figure 11. - Depletion zone formed by preferrential oxidation of Al_6Fe_6Hf precipitates in the FeAl+Hf alloy (1100 °C, cyclic).

FeAl+Zr,B, cyclic. Cyclic oxidation at 900 °C produced a whisker morphology similar to all the other 900 °C specimens and exposures. Some spall areas were noted, but the massive spallation found after isothermal exposure of this alloy did not occur after cyclic tests. Cycling to 1000 °C produced a deformed scale where, instead of smooth convolutions, discrete ridge fragments formed (Fig. 12).

At 1100 °C the spall segments were more uniformly distributed and were observed as a fine dust. However a quite singular morphology of macroscopic ridges formed (Fig. 13). These formed an array of parallel lines at approximately 45° to the longitudinal axis of the specimen. Since no underlying crystallographic or microstructural texture of the alloy existed, this phenomenon is not believed to result from any epitaxial growth mechanism. Rather it appears to be the result of large biaxial thermal expansion mismatch stresses between the alloy and scale, whose maximum shear components lie along two 45° directions. Some bidirectionality can also be discerned in the microscopic rumpling that occurred after isothermal oxidation (Fig. 8a).

1000 °C, CYCLIC

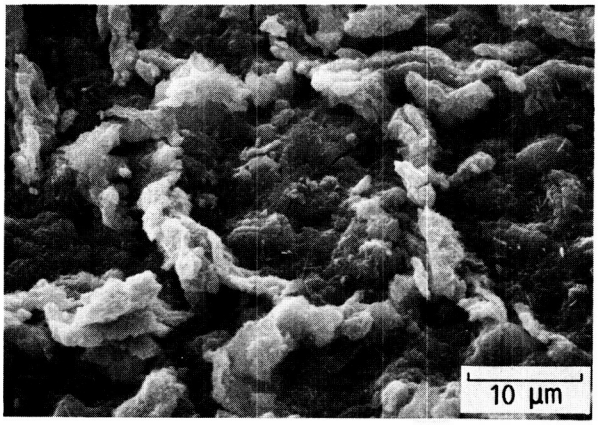

FRAGMENTED SCALE

Figure 12. - Fragmented ridges formed on FeAl+Zr,B (1000 °C, cyclic).

1100 °C, 200 1-HR CYCLES; FeAl+ZrHf

Figure 13. - Aligned macroscopic ridges formed on FeAl+Zr,B (1100 °C, cyclic).

Cyclic exposure at 1100 °C, like those of the lower temperatures, exhibited little spallation to bare metal after 200 1-hr cycles. This is in contrast to the massive spalling to bare metal that occurred for FeAl+Zr,B after isothermal oxidation at all temperatures. It appears as though the interfacial strength has been increased by continued cycling, spalling, and fragmentation of the scale. This effect is noted in the FeAl+Zr,B weight change curve in Fig. 2c where spallation, more prevalent in the beginning of the test, eventually decreased. One explanation is that the scales produced by cyclic oxidation are thinner and microcracked. As such they are more compliant and less prone to spall in massive sheets compared to the isothermal scales. Secondly, less interface voids are noted for cycled samples. Another factor is that cycling may self-purge the interface of bond-weakening segregants such as sulfur, along the lines suggested for purging effects on scale adhesion for NiCrAl (11,12).

Long term oxidation resistance of these three alloys appears to be limited to temperatures below 1100 °C. This is in contrast to Ni-50Al-0.1Zr which produced a relatively flat weight change curve, gaining less than 5 mg/cm^2 after 3000 1-hr cycles to 1200 °C (4). The performance of the two alloys containing 1 percent Hf can be explained on the basis of excess dopant, in that excessive HfO_2 formation promoted large weight gains, scale cracking, and spallation. However, excessive ZrO_2 formation did not occur for the 0.1 percent Zr alloy, and the reason for poor adhesion is not apparent. The common spall fragment and dusting phenomenon observed for all three alloys in 1100 °C cyclic tests may just be a result of the large thermal expansion mismatch stresses for FeAl alloys in general.

Summary and Conclusions

Fe-40Al alloys doped with 1Hf, 1Hf+0.4B, or 0.1Zr+0.4B were isothermally and cyclicly oxidized at 900°, 1000°, and 1100 °C. The isothermal kinetics were about a factor of five times those usually observed for pure α-Al_2O_3 kinetics. Some possible explanations were the presence of trace amounts of Fe_2O_3 in solution, rumpling of the scales, and growth of HfO_2 inner layers and ZrO_2 particles. The kinetics appeared to correlate with a shift from θ-Al_2O_3 control to α-Al_2O_3 control between 900° and 1000 °C, as previously observed for NiAl+Zr and Fe-22Al. Similar morphological changes also took place, i.e., whiskers to transformation cells to ridge networks, except where severe scale rumpling took place at 1100 °C. The Zr-doped alloy spalled extensively to bare metal after isothermal oxidation at all three temperatures, not unlike NiAl+0.1Zr after 1300 °C oxidation (14).

Cyclic oxidation showed that these alloys would be limited to temperatures below 1100 °C for long term exposures. The spalling problem appears to have been accelerated by HfO_2 formation within the scales and the large thermal expansion mismatch between Al_2O_3 and FeAl. The lack of good performance of FeAl+Zr,B cannot be explained and may indicate that FeAl alloys may be intrinsically less oxidation resistant than similar NiAl alloys. The role of boron is not known; it appears to have minimal effects in cyclic oxidation, whereas it was associated with rumpled scales in isothermal oxidation.

References

1. I. Baker and D.J. Gaydosh: "Flow and Fracture of Fe-Al," Mater. Sci. Eng., 1987, vol. 96, pp. 147-158.

2. W.C. Hagel: "The Oxidation of Iron, Nickel, and Cobalt-Base Alloys Containing Aluminum," Corrosion, 1965, vol. 21, pp. 316-326.

3. B.S. Ryl'nikov, G.V. Arkhangel'skaya, and L.V. Lyubetskaya: "Oxidation Kinetics of Fe-Al Alloys," Protection Metals, 1981, vol. 17, pp. 290-291.

4. C.A. Barrett: "Effect of 0.1 at % Zr Level on the Cyclic Oxidation Resistance of β-NiAl," Oxid. Metals, 1988, in press.

5. F. Cosandey and J. Kandra: "Trace Element Effects on Ductility and Fracture of Ni-Cr-Ce Alloys," Metall. Trans. A, 1987, vol. 18, pp. 1239-1248.

6. E.M. Schulson, T.P. Weihs, I. Baker, H.J. Frost, and J.A. Horton: "Grain Boundary Accommodation of Slip in Ni_3Al Containing Boron," Acta Met., 1986, vol. 34, pp. 1395-1399.

7. D.J. Gaydosh, S.L. Draper, and M.V. Nathal: Metall. Trans. A, submitted for publication, 1988.

8. G.C. Rybicki and J.L. Smialek: "Effect of the θ to α-A_2O_3 Transformation on the Oxidation Behavior of B-NiAl, Oxid. Metals, 1988, in press.

9. J.K. Doychak, T.E. Mitchell, and J.L. Smialek: "High Temperature Oxidation of β-NiAl," Ordered Intermetallic Alloys, MRS Symp. Proc. Vol. 39, C.C. Koch, C.T. Liu, and N.S. Stoloff, eds., Materials Research Society, Pittsburgh, 1985, pp. 475-484.

10. J.L. Smialek: "Oxide Morphology and Spalling Model for NiAl," Metall. Trans. A, 1978, vol. 9, pp. 309-320.

11. J.L. Smialek: "Adherent Al_2O_3 Scales Formed on Undoped NiCrAl Alloys," Metall. Trans. A, 1987, vol. 18, pp. 164-167.

12. J.L. Smialek: "Adherent Al_2O_3 Scales Produced on Undoped NiCrAl Alloys," in Oxidation of Metals and Associated Mass Transport, M.A. Dayananda, S.J. Rothman, and W.E. King, eds., Metallurgical Society of AIME, 1986, pp. 297-313.

13. J.K. Doychak, J.L. Smialek, and C.A. Barrett: "Oxidation of Nickel-Rich Two-Phase Ni-Al Alloys," in Oxidation of High-Temperature Intermetallics, T. Grobstein and J. Doychak, eds., Metallurgical Society of AIME, 1988, in press.

NASA
National Aeronautics and Space Administration

Report Documentation Page

1. Report No.	2. Government Accession No.	3. Recipient's Catalog No.
NASA TM-101402		

4. Title and Subtitle	5. Report Date
Oxidation Behavior of FeAl + Hf,Zr,B	6. Performing Organization Code

7. Author(s)	8. Performing Organization Report No.
James L. Smialek, Joseph Doychak, and Darrell J. Gaydosh	E-4486
	10. Work Unit No. 510-01-01

9. Performing Organization Name and Address	11. Contract or Grant No.
National Aeronautics and Space Administration Lewis Research Center Cleveland, Ohio 44135-3191	13. Type of Report and Period Covered Technical Memorandum
12. Sponsoring Agency Name and Address	14. Sponsoring Agency Code
National Aeronautics and Space Administration Washington, D.C. 20546-0001	

15. Supplementary Notes

Prepared for the Workshop on the Oxidation of High-Temperature Intermetallics sponsored by the Cleveland Chapter of ASM International and NASA Lewis Research Center in cooperation with Case Western Reserve University, The Metallurgical Society of AIME, and the Cleveland Chapter of TMS-AIME, Cleveland, Ohio, September 22-23, 1988. James L. Smialek and Darrell J. Gaydosh, NASA Lewis Research Center; Joseph Doychak, Sverdrup Technology, Inc., NASA Lewis Research Center Group, Cleveland, Ohio 44135.

16. Abstract

The oxidation behavior of Fe-40Al-1Hf, Fe-40Al-1Hf-0.4B, and Fe-40Al-0.1Zr-0.4B (at %) alloys was characterized after 900, 1000, and 1100 °C exposures. Isothermal tests revealed parabolic kinetics after a period of transitional θ-alumina scale growth. The parabolic growth rates for the subsequent α-alumina scales were about five times higher than those for NiAl + 0.1Zr alloys. The isothermally grown scales showed a propensity toward massive scale spallation due to both extensive rumpling from growth stresses and to an inner layer of HfO_2. Cyclic oxidation for 200 1-hr cycles produced little degradation at 900 or 1000 °C, but caused significant spallation at 1100 °C in the form of small segments of the outer scale. The major difference in the cyclic oxidation of the three FeAl alloys was increased initial spallation for FeAl + Zr,B. Although these FeAl alloys showed many similarities to NiAl alloys, they were generally less oxidation resistant. It is believed that this resulted from nonoptimal levels of dopants and larger thermal expansion mismatch stresses.

17. Key Words (Suggested by Author(s))	18. Distribution Statement
FeAl Oxidation Al_2O_3 scales	Unclassified – Unlimited Subject Category 26

19. Security Classif. (of this report)	20. Security Classif. (of this page)	21. No of pages	22. Price*
Unclassified	Unclassified	14	A03

*For sale by the National Technical Information Service, Springfield, Virginia 22161